Aerosol Monitoring Using a Scanning Spectral Radiometer in Sendai, Japan

By Masataka Shiobara

Meteorological Research Institute, Tsukuba, Ibaraki 305, Japan

Tadahiro Hayasaka, Teruyuki Nakajima

and

Masayuki Tanaka

Research Center for Atmospheric and Oceanic Variations, Tohoku University, Sendai 980, Japan
(Manuscript received 3 August 1990, in revised form 15 November 1990)

Abstract

Measurements of direct solar irradiance and sky radiance were carried out in Sendai, Japan for the period from September 1981 to May 1985 using a scanning spectral radiometer (aureolemeter). Size distributions of columnar total aerosols were retrieved by inverting both spectral optical thickness and solar aureole radiance data.

The size distribution of aerosols due to the El Chichon eruption in 1982 was estimated as the difference between columnar volume spectra before and after the eruption. The results indicate that the El Chichon aerosol had a monomodal volume spectrum with a mode radius about 0.5 μm; their contribution to the total aerosol volume reached the maximum in the winter of 1983, *i.e.* December 1982 to February 1983, then gradually decaying to the normal level prior to the eruption by the spring of 1985.

A seasonal model of tropospheric aerosols over Sendai was constructed by subtracting the volume spectrum of the El Chichon aerosol model from that of the columnar total aerosols, and successfully represented by a bimodal log-normal function. The aerosols in spring and summer seasons have different features in respect of volume spectra. The coarse particle mode aerosols with radii around 3 μm are predominant in spring while the accumulation mode aerosols with radii around 0.2 μm are predominant in summer.

1. Introduction

Aerosols suspended in the atmosphere have a potential to affect the radiation budget of the earth and the global climate change through change in their optical properties (Yamamoto and Tanaka, 1972; Coakley *et al.*, 1983; Coakley and Cess, 1985), and through their activity as cloud condensation nuclei (Twomey *et al.*, 1984; Wigley, 1989). Observations and modeling of the optical thickness, size distribution and refractive index of aerosols, and investigation of their spatial and temporal variations are indispensable for an assessment of the influence of aerosols on climate. Several methods for retrieving the size distribution of aerosols from the spectral optical thickness obtained by the sunphotometry have been developed and extensively employed after the first proposed by Yamamoto and Tanaka (1969). It is known, however, that the retrieved particle size is generally restricted to a narrow range because of the spectral limitation of the optical thickness measurements. Retrieval of aerosols with larger radii requires longer wavelengths. Several improved inversion methods combining the spectral extinction and scattering phase function of aerosols were thus developed and successfully applied to observed data (Green *et al.*, 1971; Twitty *et al.*, 1976; Shaw, 1979; Deepak *et al.*, 1980; Nakajima *et al.*, 1983, 1986a, b; Quenzel and Thomalla, 1987; Tanre *et al.*, 1988).

In order to obtain a long-term data set of the columnar volume spectrum of aerosols, we performed spectral measurements of solar radiation at Aobayama (38°15′N, 140°51′E, 153 m above MSL)

in the suburbs of Sendai, Japan for the period from September 1981 to May 1985. A multi-wavelength almucantar-scanning radiometer (hereafter referred to as "aureolemeter") was developed to measure both direct and scattered solar irradiance. Spectral optical thicknesses were obtained from direct solar irradiance measurements. Volume size distributions of columnar total aerosols were estimated by inverting both the spectral optical thickness and angular distributions of the solar aureole radiance with an algorithm of Nakajima *et al.* (1983, 1986a).

The optical thickness and size distribution of aerosols thus obtained can be decomposed into those of stratospheric and tropospheric aerosols. Within the observation period, the volcano El Chichon located in southern Mexico (17°20′N, 93°12′W) erupted on March 28 and then irregularly until May 1982. In the present study, size distributions of stratospheric aerosols due to the El Chichon eruption were estimated as a difference between columnar size distributions before and after the eruption. After investigating the results and referring to previous studies on El Chichon aerosols (Knollenberg and Huffman, 1983; Oberbeck *et al.*, 1983; Hofmann and Rosen, 1984; Michalsky *et al.*, 1984; Asano *et al.*, 1985; Spinhirne and King, 1985; Nakajima *et al.*, 1986a), we constructed a model of stratospheric aerosols pertaining to the period after the El Chichon eruption. Size distributions of tropospheric aerosols (including the background stratospheric aerosols in the strict sense) were also derived by subtracting the modeled distribution of the El Chichon aerosols from the columnar total aerosol distributions. We present further a seasonal model of tropospheric aerosols over Sendai, and discuss its seasonal features.

2. Design of the aureolemeter

We have developed an aureolemeter which can measure not only direct solar irradiance but sky radiance in the solar almucantar. The aureolemeter is equipped with a silicon photodiode and five interference filters at wavelengths of 369, 500, 675, 776 and 862 nm as illustrated in Fig. 1. The filter wheel rotates at 375 rpm in front of the detector. The detector produces an output current, which is proportional to the magnitude of incident irradiance and amplified by a linear current/voltage converter with a dynamic range of 10^5. The output voltage is separated into signals corresponding to each wavelength by means of a sample-and-hold circuit. A significant advantage of this circuit is an improvement of the S/N ratio since the drift of the dark current from the detector is canceled out. The aureolemeter with a field-of-view (FOV) of 1° can be aimed at any direction along the solar almucantar by a DC servo-motor. Calibration of the aureolemeter was carried out several times every year with the improved Langley method proposed by Tanaka *et al.* (1986).

Precise measurements of the solar aureole at small scattering angles from the sun are quite important because such measurements enable the retrieval of aerosol size distribution in wider radius ranges (Takamura and Tanaka, 1985). The finite FOV of the instrument as well as that of solar disk (Box and Deepak, 1981), however, seriously affects the retrieval of the phase function of aerosols because of its large growth rate with decreasing scattering angle. We estimated errors involved in the retrieved phase function due to the finite FOVs of the instrument and the sun based on a single scattering approximation, and determined a desirable FOV angle for the aureolemeter. It is found from the discussion in Appendix that we can obtain the phase function with an accuracy better than 2 % for scattering angles larger than 1° if the half (full) angle of FOV of the aureolemeter is designed to be smaller than 0.5° (1.0°).

The following considerations were also taken into account in the design of aureolemeter:

(1) Sun-shade baffles in front of the object lens are indispensable for preventing stray light contamination due to the reflection of solar radiation in the aureolemeter. These baffles were designed to enable us to measure the aureole irradiance for scattering angles greater than 1.25°.

(2) The optical alignment should be made to keep the incident angle to the filters as small as possible since the peak wavelength of incident radiation transmitted through the interference filters shifts depending on the incident angle.

(3) The temperature of the detector should be controlled to a temperature of 40°C±1°C to negate any errors due to the temperature dependence of the detector's sensitivity.

Specifications of the aureolemeter are summarized in Table 4 of Tanaka *et al.* (1986)

3. Observations and data analysis

Spectral measurements of solar radiation were performed at Aobayama (38°15′N, 140°51′E, 153 m above MSL) in the suburbs of Sendai, Japan from September 1981 to May 1985. Aobayama, which is located to the west of Sendai city, neighbors with the Owu Mountains (1500–1800 m above MSL) in the northwest and with the Pacific Ocean in the southeast as shown by Fig. 2. The aureolemeter was set up on the rooftop of a research building in the Aobayama campus of Tohoku University. Measurements were carried out on cloudless days in the following manner. At first, the direct solar irradiance was measured for wavelengths of 369, 500, 675, 776 and 862 nm. Subsequently the scattered radiance was measured along the solar almucantar by scanning from the sun. Fifteen azimuth angles between

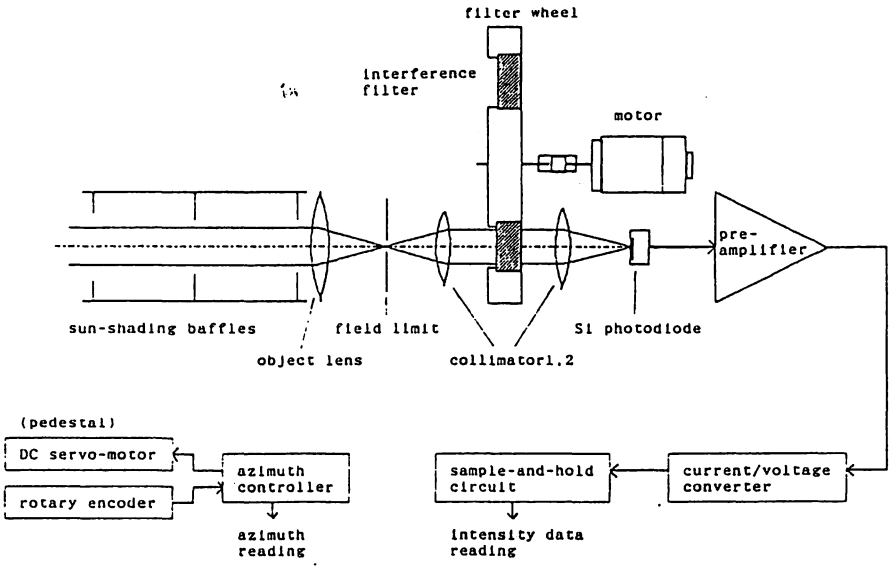

Fig. 1. Optical alignment and outline of electrical circuits of the aureolemeter.

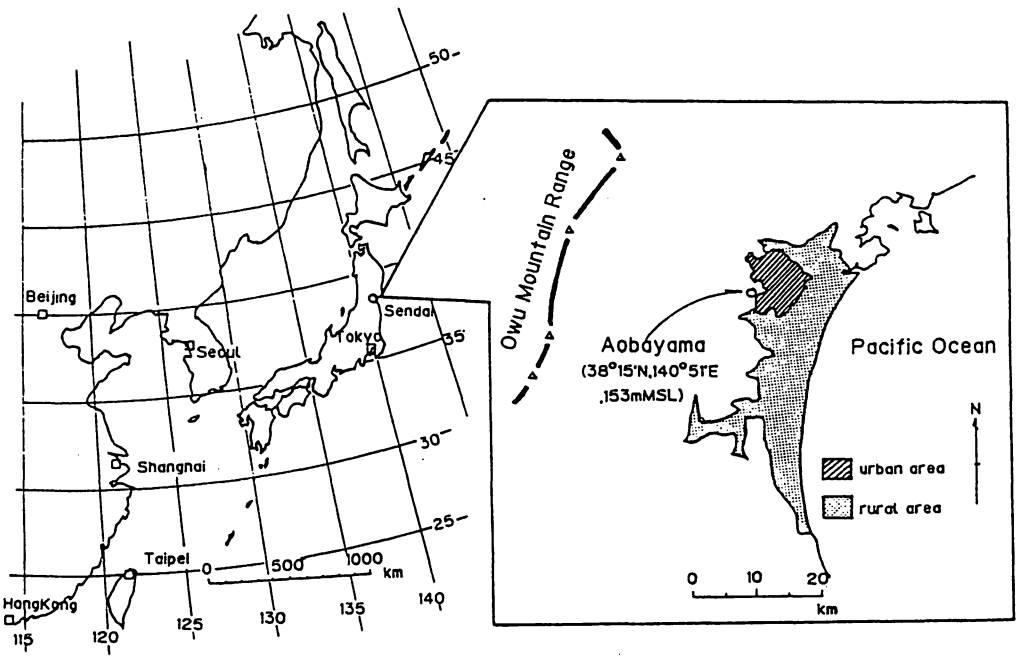

Fig. 2. Location of the observation site at Aobayama in the suburbs of Sendai, Japan.

1.25° and 180° were selected depending on the solar elevation so that the scattering angles range from 1.25° to 60°. It takes 8 minutes for a complete measurement of the direct and aureole radiances at the five wavelengths. In order to ascertain the homogeneity of atmospheric condition around the sun, the aureolemeter scanned to the right and left from the sun. If the measured radiances between the right and left scans were different by more than 5 %, those data were excluded from the succeeding analyses.

The optical thickness of aerosols $\tau_a(\lambda)$ at wavelength λ is evaluated by subtracting the optical thicknesses due to molecular scattering $\tau_m(\lambda)$ and gaseous absorption $\tau_g(\lambda)$ from the total optical thickness $\tau_t(\lambda)$ using the relationship,

$$\tau_a(\lambda) = \tau_t(\lambda) - \tau_m(\lambda) - \tau_g(\lambda). \quad (1)$$

$\tau_t(\lambda)$ is obtained from the direct solar irradiance $F(\lambda)$ measured on the ground and $F_o(\lambda)$ at the top of the atmosphere by the following equation:

$$\tau_t(\lambda) = \ln\left(F_o(\lambda)/F(\lambda)/D^2\right)/m, \quad (2)$$

where m is the optical airmass and D is the distance between the sun and the earth in astronom-

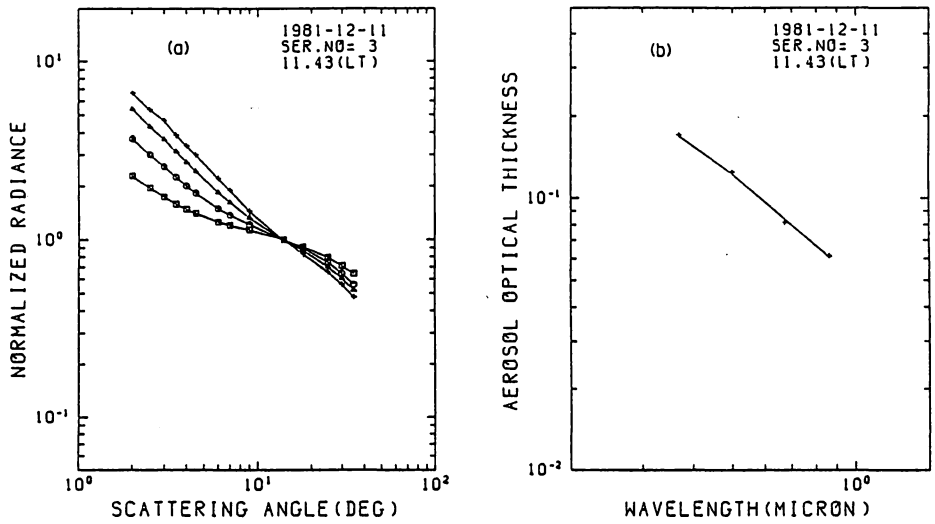

Fig. 3. (a) Angular distributions of the aureole radiance at wavelengths of 369 (rectangles), 500 (circles), 675 (triangles) and 862 nm (crosses), respectively, measured on December 11, 1981. The radiance is normalized by the value at the scattering angle of 15°. (b) Spectral optical thickness of aerosols. Crosses and a line indicate values from the measurement and those reconstructed from the volume spectrum presented in Fig. 5, respectively.

ical units. $\tau_m(\lambda)$ is estimated by the formula proposed by Fröhlich and Shaw (1980). The absorption by ozone (Chappuis band) is taken into account for $\tau_g(\lambda)$ at λ=500 nm and 675 nm. An average of the column amounts of ozone at Tateno and Sapporo observed by the Japan Meteorological Agency was used for the value at Sendai. We adopted the ozone absorption coefficient of CIAP (1975).

Figure 3 shows, for example, the angular distributions of aureole radiance and spectral distribution of $\tau_a(\lambda)$ at λ=369, 500, 675, 862 nm, which were measured on December 11, 1981. In this study, we did not use the data of λ=776 nm because these optical thicknesses frequently showed unexpected large values even after a correction for the effect of oxygen A-band absorption. An iterative algorithm developed by Nakajima *et al.* (1983, 1986a) was used for retrieving the size distribution of aerosols from those measurements. In this algorithm, the procedure is divided into two steps, *i.e.* estimation of the scattering phase function of aerosols by removing a theoretical estimate of the multiple scattering radiance from the aureole data, and estimation of a volume spectrum by inverting the optical thickness and phase function of aerosols. The aerosol optical thickness $\tau_a(\lambda)$ is given by

$$\tau_a(\lambda) = \int_{-\infty}^{\infty} K_e(\lambda, \ln r) \frac{dV}{d\ln r} d\ln r. \quad (3)$$

The scattering phase function $\beta_\lambda(\Theta)$ at the scattering angle Θ is given by

$$\beta_\lambda(\Theta) = \int_{-\infty}^{\infty} K_{s,\lambda}(\Theta, \ln r) \frac{dV}{d\ln r} d\ln r \quad (4)$$

where $dV/d\ln r$ is the volume size distribution of aerosols, dV is the volume of aerosols contained in an interval $d\ln r$, and r is the radius of an aerosol particle. $K_e(\lambda, \ln r)$ and $K_{s,\lambda}(\Theta, \ln r)$ are the kernel functions for extinction and scattering, respectively derived from Mie scattering theory. Normalized kernel functions for extinction and scattering versus the size parameter, $2\pi r/\lambda$, are illustrated in Fig. 2 of Nakajima *et al.* (1986a) We solve these equations as a simultaneous inverse problem to obtain the volume spectrum $dV/d\ln r$.

The procedure starts from an initial condition where a power law size distribution of aerosols is assumed. The doubling method was used for calculating the radiation transfer or estimating the multiple scattering in the atmosphere above the surface whose albedo was assumed to be 0.15. Calculations were repeated until the r.m.s. difference between the calculated and observed radiances becomes less than 0.1 % or until the r.m.s. difference between those at the $(n-1)$th iteration and the n-th iteration becomes less than 0.01 %. Most of the inversions terminated after a 5–6 times iteration by the latter criterion. The r.m.s. difference exceeding 10 % at the beginning of iterations decreased successfully to 2–3 % at the final iteration, as shown by Fig. 4. This confirms that the observed data can be reconstructed in a highly consistent manner by radiation transfer theory assuming a plane parallel atmosphere and spherical particles.

Through this procedure, we finally obtained the volume spectrum, for example shown in Fig. 5 from data shown in Fig. 3. Tanaka *et al.* (1982) found that the volume spectrum can be retrieved without large uncertainties if the maximum contribution of

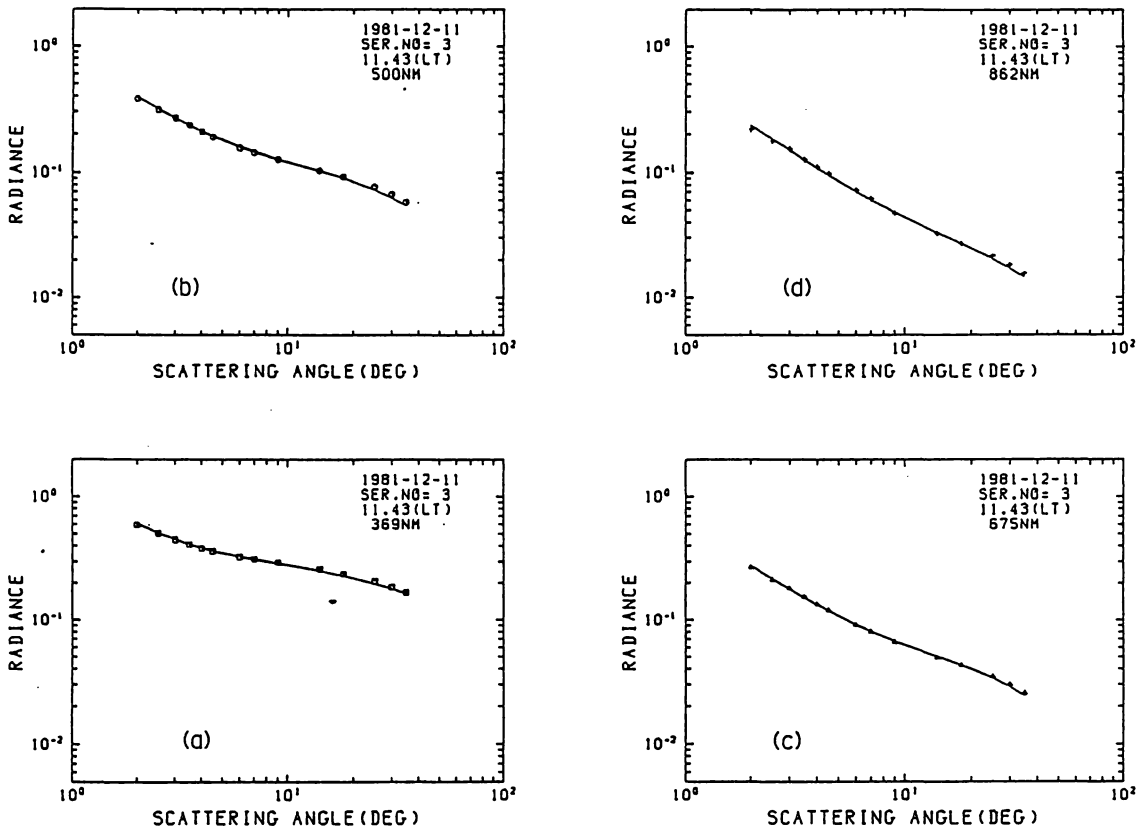

Fig. 4. Comparisons of aureole radiances between observed (symbols) and reconstructed (curves) values at wavelengths of 369 (a), 500 (b), 675 (c) and 862 nm (d), respectively, from the measurement presented in Fig. 3.

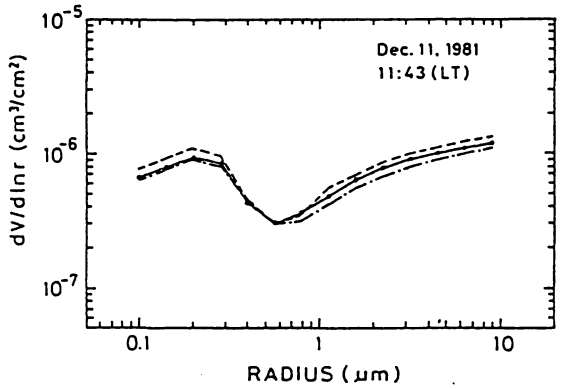

Fig. 5. Volume size spectra of columnar total aerosols retrieved from data indicated in Fig. 3, assuming the refractive index of aerosols to be 1.5–0.01i (solid curve with solid circles), 1.45–0i (broken curve) and 1.5–0.03 (dot-broken curve).

the spectrum at a particular radius range to any part of observed data, C_{max}, safely exceeds the r.m.s. error of the data. The error of the measured data, which includes the specific error of the aureolemeter as well as observational errors, is at most 5 % so that the radius range where the value of C_{max} exceeds 5 % in the inversion procedure is expected to be reliable. The reliable range was extended over 0.2–8 μm in most cases of this study. Consequently, it is found that the optical thickness data are responsible for the small size range of size distribution retrievals while the aureole data are responsible for the large size range (Nakajima *et al.*, 1983; Tanaka *et al.*, 1989).

In the present analysis, the refractive index of aerosols is assumed to be 1.5–0.01i, which is considered to be an average for tropospheric aerosols except for that in urban areas (Tanaka *et al.*, 1983; WMO, 1983). We added in Fig. 5 the other solutions of retrieval assuming the refractive indices of 1.45–0i (broken curve), which is more suitable for non-light-absorbing particles such as sulphates or sulfuric acid aerosols, and 1.5–0.03i (dot-broken curve), which is suitable for light-absorbing particles such as carbon-rich or urban aerosols. Comparisons among those three curves indicate that the present retrieval method does not depend strongly on the assumed refractive index. This is because the extinction cross section and the forward scattering cross section of aerosols are not sensitive to detailed values of the aerosol refractive index. Hence columnar size distributions retrieved in this analysis may not contain large errors even in the enhanced stratospheric aerosols case.

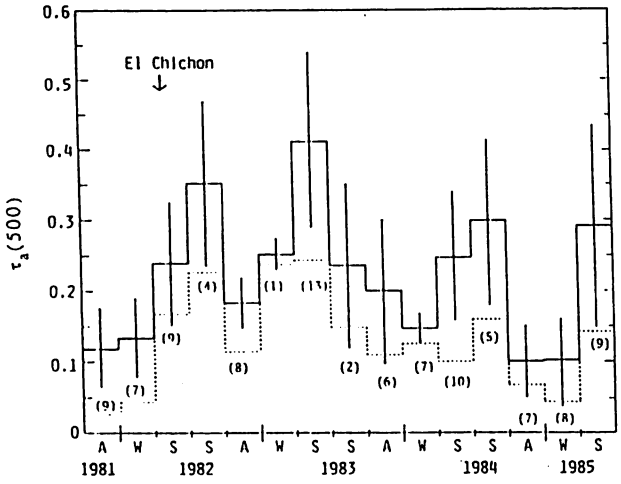

Fig. 6. Temporal variation of the aerosol optical thickness at λ=500 nm, τ_a(500). Seasonal average values and r.m.s. deviations are indicated by solid-step and vertical lines, respectively. The broken-step line indicates the minimum value in each season. Parenthesized numerics in each season indicate the number of days of observation.

4. Results and discussion

a. Temporal variation of columnar total aerosols

The aerosol optical thickness was derived from the direct solar irradiance measured on 104 days in the observation period. Figure 6 shows the temporal variation of aerosol optical thickness at λ=500 nm, τ_a(500), averaged seasonally. Here τ_a(500) for averaging are only those used for retrieving the volume spectra. A seasonal variation of τ_a(500) is found with a large day-to-day variation. The average values (solid-step line in Fig. 6) are large in spring (defined as March 1 to May 31) and summer (June 1 to August 31), but are small in autumn (September 1 to November 30) and winter (December 1 to February 28/29). The variations in τ_a(500), which are represented by vertical bars as the r.m.s. of seasonal values in Fig. 6, are large with deviations of about 50% of the seasonal mean value for all the year. A long-term variation in τ_a(500) is also found with the maximum in the spring of 1983. Comparing the average values of each season, it is found that seasonal averages in the period from the summer of 1982 to the spring of 1983 are larger by 0.05–0.15 than those of the same seasons in other periods. The minimum value of τ_a(500) observed in each season also shows the similar variation (broken-step line in Fig. 6), *i.e.* they increased noticeably from the spring of 1982 to the spring of 1983, and decreased gradually with time until 1985. τ_a(500) in 1985 returned to a comparable level to that in 1981. This observation means that the variation of τ_a(500) revealed in this study consists of a long-term variation due to stratospheric aerosols as a bias and a short-term variation due to tropospheric aerosols. Compared with the height-integrated backscattering coefficient of the stratospheric aerosols observed in Japan by lidars (Uchino *et al.*, 1984; Hayashida and Iwasaka, 1985), the long-term variation of τ_a(500) seems to suggest an increase and decline of the volcanic aerosols in the stratosphere due to the El Chichon eruption. Asano *et al.* (1985) reported the increase in τ_a(500) due to the El Chichon aerosols of 0.17 in December 1982 and 0.09 in January 1983 at Tsukuba, Japan (*i.e.*, the differences of the optical thickness from the preceding year). Also at Sendai, τ_a(500) in the winter of 1983 (*i.e.*, December 1982 to February 1983) was about 0.1 larger than that in the winter of 1982, as shown by Fig. 6.

168 sets (one set contains data of spectral optical thicknesses and aureole radiances at the four wavelengths) of data measured on 104 days (*i.e.*, 1–4 sets a day) were analyzed to retrieve the volume spectrum of aerosols. Retrieved size distributions of columnar aerosols are summarized for the respective seasons from the autumn of 1981 to the spring of 1985 in Fig. 7. Seasonal average values and r.m.s. deviations of the retrieved size spectra are indicated by solid and broken curves, respectively. Typically, bimodal spectra were observed before the summer of 1982, whereas monomodal spectra with a mode radius near 0.5 μm were evident during the period from the autumn of 1982 to the spring of 1984. The monomodal distribution disappeared after the summer of 1984, and a Junge-type (*i.e.*, power law distribution) or a weak bimodal distribution predominated. Such an extended temporal variation of size distribution suggests that the El Chichon stratospheric aerosol loading was high, and largely modified the size distribution of the columnar total aerosols in the period from the autumn of 1982 to the spring of 1984.

b. The El Chichon aerosols

The volume spectra of aerosols due to the El Chichon eruption were estimated for the autumns of 1982, 1983 and 1984, and the winters of 1983, 1984 and 1985, by subtracting those of corresponding seasons prior to the El Chichon eruption. The reason why only autumn and winter are chosen is that the error in subtracting El Chichon aerosols is expected to be small in those seasons when the tropospheric aerosol loading is generally small. The results in Fig. 8 show that aerosols of El Chichon origin had monomodal volume spectra with a mode radius of about 0.5 μm. These volume spectra are in good agreement with those observed around northern hemisphere mid-latitudes retrieved from ground-based solar irradiance measurements (Michalsky *et al.*, 1984; Asano *et al.*, 1985) and from direct and indirect airborne measurements (Knollenberg and

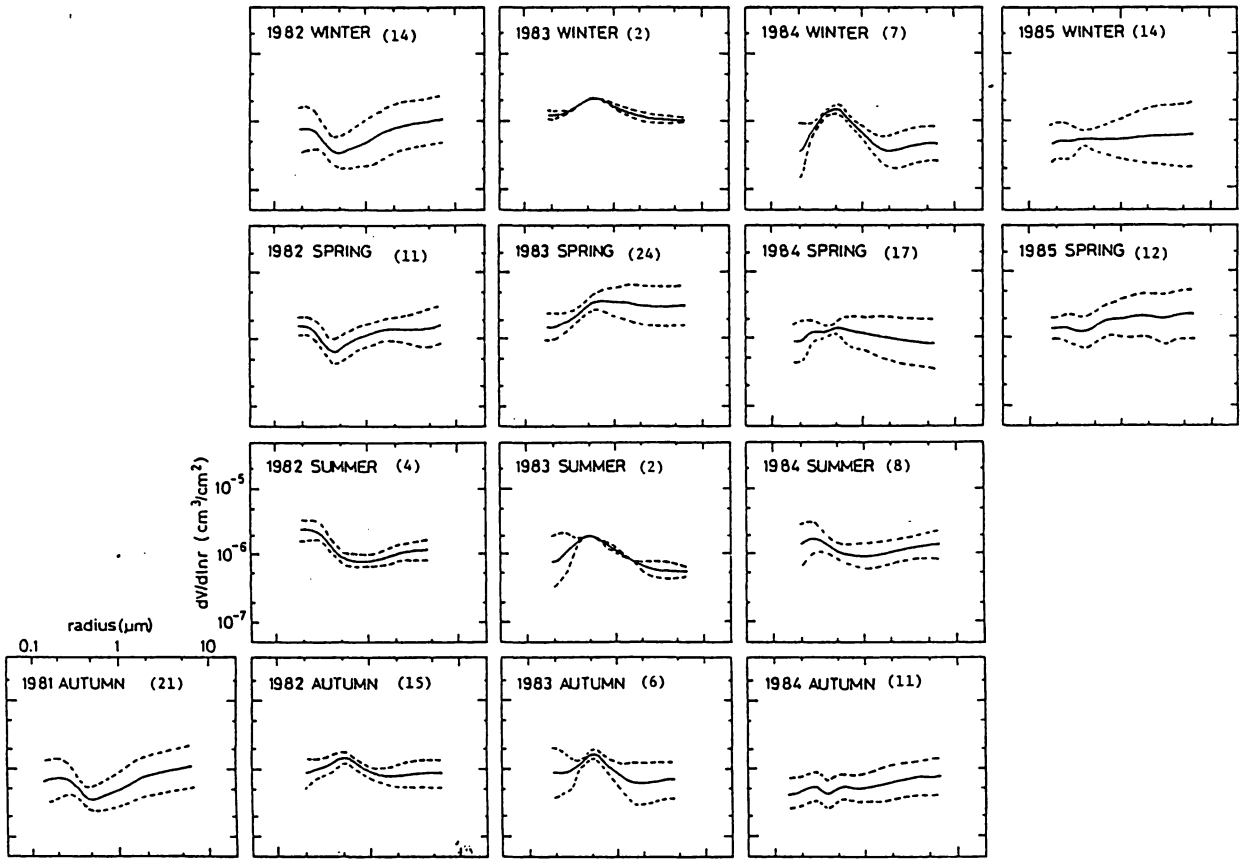

Fig. 7. Seasonal average values (solid curves) and r.m.s. deviation (broken curves) of the volume spectra of columnar total aerosols in the respective seasons from the autumn of 1981 to the spring of 1985. Parenthesized numerics in each panel indicate the number of retrieved volume spectra.

Huffman, 1983; Oberbeck *et al.*, 1983; Hofmann and Rosen, 1984; Spinhirne and King, 1985; Nakajima *et al.*, 1986a).

Airborne samples of aerosols in the stratosphere and their component analysis with scanning electron microscopy and energy dispersive X-ray spectroscopy were carried out by several investigators after the eruption of El Chichon (*e.g.* Gooding *et al.*, 1983; Woods and Chuan, 1983). They indicated that stratospheric aerosols were dominated by magmatic and lithic particles larger than about 3 μm in diameter and were distributed between latitudes 10°N and 60°N, but concentrated mainly at latitudes between 13°N and 30°N until July, 1982. In October 1982, the aerosols dispersed uniformly from 10°S to 75°N, changing their composition into more complex structures such as ash particles and sulfuric acid droplets. In November and December 1982, the largest particles found were about 4 μm in diameter, as a result of the gravitational fall-out, and the remaining small particles were mostly made of sulfuric acid. The small particles made by gas-to-particle conversion processes require a long time for further growth of particles by condensation and coagulation. For instance, Shibata *et al.* (1984) simulated the evolution of stratospheric aerosols with an initial condition of injection of sulfur dioxide gas from the volcanic eruption. Nine months was estimated as the time for the formation of particles with a mode radius of about 0.33 μm.

In Fig. 9, we summarize the relationship between the volume mode radius of aerosols and elapsed time after the eruption, using previously reported values (Knollenberg and Huffman, 1983; Oberbeck *et al.*, 1983; Hofmann and Rosen, 1984; Michalsky *et al.*, 1984; Asano *et al.*, 1985; Spinhirne and King, 1985; Nakajima *et al.*, 1986a) and a model of nonvolatile aerosols from the Agung (8°25'S, 115°30'E) eruption in 1963 (Mossop, 1964; Toon and Pollack, 1976). Original size distributions reported in those literatures were converted, if necessary, to volume spectra in order to compare consistently with our results. This figure suggests that magmatic ash particles with a large mode radius due to such volcanic eruption as the Agun were dissipated by gravitational sedimentation, whereas the secondarily produced particles increased in radius up until a submicron mode. With respect to the dissipation of the secondary particles from the stratosphere, Post (1986) pointed out that these particles, contrary to the primary large particles, are removed not by the gravitational fall-out but by frontal folding pro-

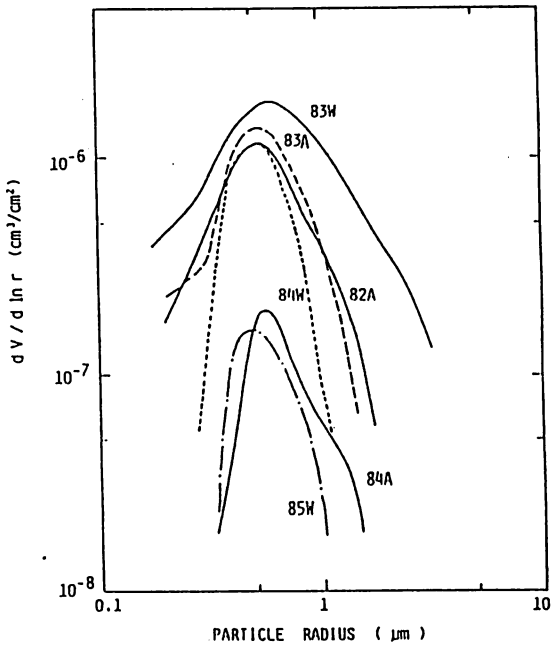

Fig. 8. Size distribution anomalies estimated as a residual of the volume spectrum of columnar total aerosols retrieved after the El Chichon eruption against that of the corresponding season previous to the eruption.

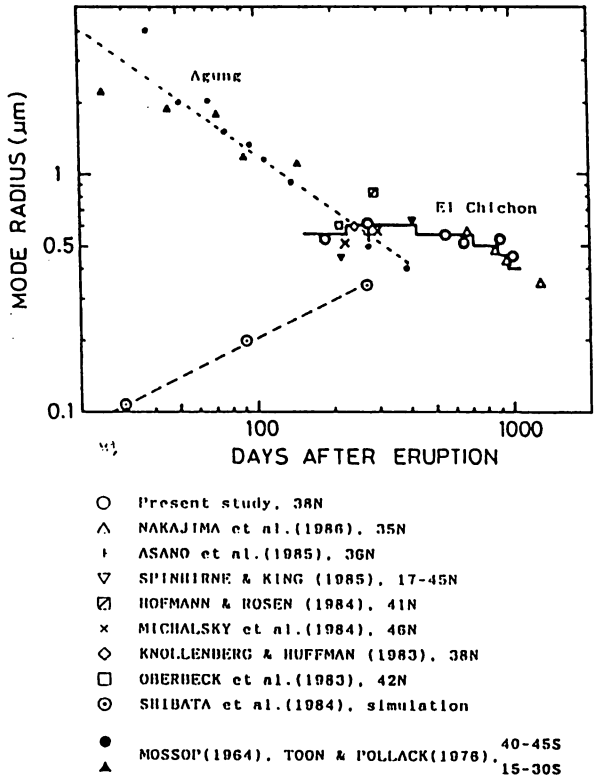

Fig. 9. The relationship between the mode radius of stratospheric aerosols due to volcanic origin and days elapsed after the eruption. All of those except for the result calculated by Shibata *et al.* (1984) are derived from observations at the latitude given after the author's name.

cesses. From the above discussion, it is inferred that the size distribution of aerosols due to the El Chichon eruption, especially that after the autumn of 1982, was made of evolving sulfuric particles.

Referring to the results of several investigations presented above and Figs. 8 and 9, we derived a model of the size distribution of stratospheric aerosols due to the El Chichon eruption for the period from the autumn of 1982 to the winter of 1985. The volume spectrum of those aerosols, $dV/d\ln r$, is expressed by a log-normal distribution given by

$$dV/d\ln r = C \cdot \exp\left\{-((\ln r - \ln a)/\ln s)^2/2\right\}, \quad (5)$$

where C, a and s are parameters related to concentration, mode radius and dispersion of the log-normal volume spectrum respectively, which were derived for individual spectra from best fit by eyes and then seasonally averaged for each season as summarized in Table 1. The values for spring and summer in the period were smoothly interpolated in time between the winter and autumn values. The temporal variation of the seasonal average of a is indicated by a solid-step line in Fig. 9. Total volumes of the El Chichon aerosols, V in Table 1, were derived by integrating the volume spectra over the radius range from 0.1 to 10 μm. Model values of $\tau_a(500)$ and the ratio V/τ_a are also tabulated there.

Figure 10 shows the temporal variation of the total volume of the El Chichon aerosols modeled by Eq. (5), compared with those estimated from Fig. 8 and from the results of other studies (Michalsky *et al.*, 1984; Asano *et al.*, 1985; Nakajima *et al.*, 1986a). Since those volumes in Fig. 10 were derived by integrating over the radius range 0.2–2 μm to make a consistent comparison with the results of other researchers, the volumes thus estimated may be underestimated by more or less 5%. It is inferred that the total volume of secondarily produced stratospheric aerosols after the El Chichon eruption increased to $2\text{–}3\times10^{-6}$ (cm^3/cm^2) in the winter of 1983 and then decreased with an e-folding time of 200–250 days until 1985. In the winter of 1985, the El Chichon aerosol volume decreased to 1×10^{-7} (cm^3/cm^2) and $\tau_a(500)$ decreased to less than 0.01 which is comparable to that in the normal stratosphere, so that the stratosphere returned to the normal state, which could not be distinguished from that prior to the eruption by ground-based measurements, in the spring of 1985.

In a practical way, the value of V/τ_a can be assumed to be 2.5×10^{-5} in the enhanced stage of the El Chichon aerosols and 2×10^{-5} in their decay stage in order to estimate the total aerosol volume from optical thickness measurements.

Table 1. Parameters C, a and s used in Eq. (5) for modeling El Chichon aerosols.

Seasons		C (cm^3/cm^2)	a (μm)	s	V (cm^3/cm^2)	τ_s	V/τ_s
1982	Autumn	8.0×10^{-7}	0.55	1.50	8.13×10^{-7}	0.036	2.26×10^{-5}
1983	Winter	1.8×10^{-6}	0.60	1.50	1.83×10^{-6}	0.072	2.55×10^{-5}
	Spring	1.5×10^{-6}	0.60	1.50	1.53×10^{-6}	0.060	2.55×10^{-5}
	Summer	1.4×10^{-6}	0.55	1.50	1.42×10^{-6}	0.056	2.26×10^{-5}
	Autumn	1.2×10^{-6}	0.55	1.50	1.22×10^{-6}	0.048	2.26×10^{-5}
1984	Winter	1.0×10^{-6}	0.55	1.50	1.02×10^{-6}	0.040	2.26×10^{-5}
	Spring	7.0×10^{-7}	0.50	1.50	7.11×10^{-7}	0.036	1.99×10^{-5}
	Summer	3.0×10^{-7}	0.50	1.50	3.05×10^{-7}	0.015	1.99×10^{-5}
	Autumn	2.0×10^{-7}	0.45	1.50	2.03×10^{-7}	0.012	1.74×10^{-5}
1985	Winter	1.0×10^{-7}	0.40	1.50	1.02×10^{-7}	0.007	1.52×10^{-5}

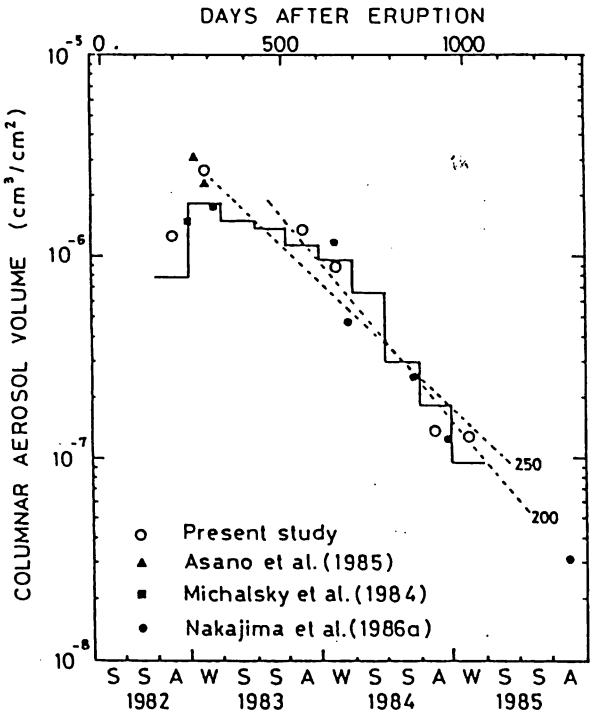

Fig. 10. Temporal variations of the total volume of the El Chichon aerosols modeled (solid-step line), those observed by the present study (open circles), by Nakajima *et al.* (1986, closed circles), by Asano *et al.* (1985, closed triangles) and by Michalsky *et al.* (1984, closed rectangles).

c. Tropospheric aerosols

Tropospheric aerosols are frequently described by a bimodal volume size distribution, *i.e.* a coarse particle mode with a mode radius of the order of microns and an accumulation mode with a mode radius of the order of sub-microns (Whitby *et al.*, 1972; Patterson and Gillette, 1977; Nakajima *et al.*, 1986b; Kim *et al.*, 1988; Hayasaka *et al.*, 1990). Such a size distribution results from production, condensation, coagulation, and transport and removal processes. The Aitken nuclei are produced through gas-to-particle conversion and combustion processes. These small particles increase in size by condensation and coagulation, and constitute the accumulation mode. The coarse particle mode aerosols in the maritime planetary boundary layer consist mainly of sea salt particles which are produced by bursting bubbles at the ocean surface (Woodcock *et al.*, 1953; Knelman *et al.*, 1954; Toba, 1959). On the other hand, those in the continental planetary boundary layer mainly consist of wind blown soil particles (Patterson and Gillette, 1977). The removal processes, such as gravitational sedimentation and rain-out, are also important for the structure of size distribution of tropospheric aerosols. Since the roles of production, growth, transport and removal processes on the tropospheric aerosol loading are different both spatially and temporally, their size distributions have a wide variety in the space-time domain, although the bimodal structure itself still remains.

In this study, the volume spectra of tropospheric aerosols were estimated by subtracting the modeled volume spectra of El Chichon aerosols (via Eq. (5) and Table 1) from those of columnar total aerosols. The contribution of the background stratospheric aerosol amount to the total amount is so small that almost all of the columnar aerosols consist of tropospheric aerosols for the periods except the El Chichon event., For example, $\tau_a(500)$ of stratospheric aerosols for the non-El Chichon periods is about 0.02 or less (Nakajima *et al.*, 1986a; Tanaka *et al.*, 1990) so that the contribution of the background stratospheric aerosols to the columnar total aerosols is expected to be small.

We fitted a bimodal log-normal function to the volume spectrum estimated above, using the least squares method:

$$dV/d\ln r = \sum_{i=1}^{2} C_i \cdot \exp\left\{-((\ln r - \ln a_i)/\ln s_i)^2/2\right\}, \quad (6)$$

Table 2. Parameters C_1, C_2, a_1, a_2, s_1 and s_2 used in Eq. (6) for modeling tropospheric aerosols.

Seasons	Winter	Spring	Summer	Autumn
C_1 (10^{-6} cm^3/cm^2)	0.89±0.39	1.71±0.77	2.65±0.86	0.97±0.66
a_1 (μm)	0.16±0.04	0.17±0.05	0.21±0.04	0.15±0.05
s_1	1.79±0.19	1.69±0.25	1.97±0.16	1.96±0.48
C_2 (10^{-6} cm^3/cm^2)	1.19±0.76	3.35±2.18	1.28±0.42	1.05±0.43
a_2 (μm)	4.48±1.62	2.78±1.60	2.98±0.98	3.96±1.70
s_2	3.47±1.24	3.06±0.89	2.17±0.37	3.12±0.84
V (cm^3/cm^2)	5.01×10^{-6}	1.17×10^{-5}	6.99×10^{-6}	4.61×10^{-6}
τ_a	0.12	0.28	0.33	0.13
V/τ_s	4.12×10^{-5}	4.20×10^{-5}	2.13×10^{-5}	3.65×10^{-5}

where C_i, a_i and s_i are the parameters related to concentration, mode radius and dispersion of each mode of volume spectrum, respectively. Table 2 shows these parameters for the four seasons obtained by averaging seasonally the volume spectra from September 1981 to May 1985. The volume spectra modeled with these parameters are illustrated in Fig. 11.

It was found that the aerosol volume spectra in winter and autumn are similar to each other and their concentrations are lower than those in the other two seasons. On the other hand, in spring, both peaks of the accumulation and coarse particle modes are larger than those in winter and autumn. The coarse particle mode is predominant with a conspicuous variation of concentration, *i.e.* a large r.m.s. deviation of coefficient C_2. Such coarse particles are generally believed to consist of soil-derived dust or sea salt as noted earlier. The enhancement of the coarse particle mode was frequently observed during a prevailing northwesterly wind. The surface wind of Sendai from the east or south, *i.e.* from the sea, is not so predominant in spring, especially in March and April. Such a wind is observed mostly in summer, although coarse particles are not abundant in that season. Therefore, it is difficult to attribute the coarse particle mode aerosols during spring to sea salt particles. In spring, the southwestern part of Japan is often covered by a dust cloud transported from eastern Asia, known as the Yellow-sand event. Tanaka *et al.* (1989), as well as Arao and Ishizaka (1986), have observed abundant coarse particles with radii larger than 2 μm during the Yellow-sand events at Nagasaki, and suggested that a large amount of Asian dust should be expected to be occasionally evident in the troposphere over Japan. The coarse-particle mode aerosols observed in spring may be attributed to the soil-derived particles similar to those in the Yellow-sand event although the obvious events are rarely observed at Sendai.

In summer, contrary to spring, the accumulation mode is predominant while the coarse particle mode

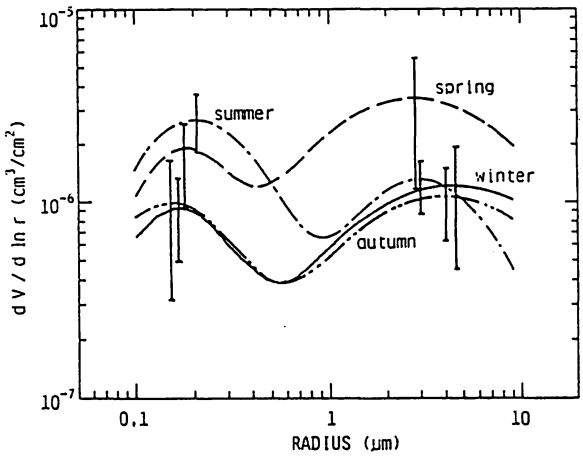

Fig. 11. The seasonal model of the tropospheric aerosol volume spectrum represented by Eq. (6) with parameters in Table 2. Modeled spectra of winter, spring, summer and autumn are drawn with solid, broken, dotted broken and double-dotted broken curves, respectively. Vertical lines indicate r.m.s. deviations of the parameters C_1 and C_2 for each season.

is rather similar to those of winter and autumn. The accumulation mode aerosols are usually found in the planetary boundary layer, while coarse-particle mode aerosols are found in and above the planetary boundary layer. (Fitch and Cress, 1981, 1983; Tanaka *et al.*, 1990; Hayasaka *et al.*, 1990). It is, therefore, reasonable to infer that the accumulation mode aerosols of summer are substances of surface origin, and grow by condensation and coagulation under high temperature and abundant water vapor conditions.

As suggested in Table 2, the seasonal features discussed above are represented consistently by the seasonal difference in the ratio V/τ_a. Dominance of the accumulation mode in summer is responsible for the smaller value of V/τ_a in summer than

in any other season. The autumn is an intermediate between summer and winter. It is interesting to note that the ratios in winter are as large as that in spring. Consequently, we can estimate the seasonal columnar total volume of aerosols from the optical thickness measurements assuming $V/\tau_a \sim 2\times10^{-5}$ in summer and 4×10^{-5} in the other seasons.

5. Summary

Spectral measurements of direct and scattered solar irradiance were carried out in Sendai, Japan, for the period from September 1981 to May 1985 with a scanning spectral radiometer (aureolemeter). The long-term variation of aerosol optical thickness was obtained from direct solar irradiance data; size distributions of columnar total aerosols were also retrieved by the iterative inversion of the spectral optical thicknesses and the solar aureole radiance distributions. The size distribution of El Chichon aerosols was estimated as the difference between columnar volume spectra before and after the eruption. From these results and the previous investigations, we made a model of volume spectra of the El Chichon aerosols fitted to a log-normal distribution. Furthermore, a seasonal model of tropospheric aerosols over Sendai was constructed by subtracting the volume spectrum of the El Chichon aerosol model from that of the columnar total aerosols, and successfully representing them with a bimodal log-normal distribution. Results of the present study are summarized as follows:

(1) Variations of optical thickness and volume spectrum of aerosols, as shown in Figs. 6 and 7, suggested that the stratospheric aerosols due to the El Chichon eruption had maximum influence on atmospheric turbidity in the winter of 1983, *i.e.* from December 1982 to February 1983, decaying to the normal level prior to the eruption by spring of 1985 over Japan. These trends are summarized in Table 1 in terms of modeled log-normal functions. It is also inferred that these monomodal aerosols with the mode radius about 0.5 μm, as shown in Fig. 8, consisted of secondarily produced particles through the gas-to-particle conversion process.

(2) Bimodal volume spectra prevail for the tropospheric aerosols over Sendai throughout a year as reported in Table 2 and Fig. 11. The aerosol optical thickness is high in both spring and summer. However, the aerosol size distributions of those seasons have different features. The coarse-particle mode aerosols, with radii around 3 μm, are predominant in spring. Aerosols contained in this mode may be attributed to the dust transported from the Asian continent. On the other hand, the accumulation mode aerosols, with radii around 0.2 μm, are predominant in summer, suggesting a large contribution of surface-origin aerosols increasing in size through condensation and coagulation processes.

These results suggest further that aureolemeters are useful for monitoring the atmospheric aerosols, especially their columnar size distribution.

Acknowledgements

The authors are grateful to Y. Nakanishi for cooperation in developing the aureolemeter, and J.D. Spinhirne of NASA Goddard Space Flight Center, S. Asano and O. Uchino of Meteorological Research Institute for valuable comments on the first draft of the paper, and further to T. Ito and anonymous referees for reviewing kindly this paper. Ozone data, indispensable for the present analysis, were provided by the Tateno Aerological Observatory.

Appendix

Estimation of errors due to finite field-of-views of the instrument and the sun

The intensity of singly scattered radiation from the direction (θ_o, ϕ_o) to the direction (θ, ϕ), with zenith angle θ and azimuth angle ϕ, is given as

$$I(\mu, \mu_0, \phi - \phi_0) = I_o\bar{\omega}_o P(\Theta)(e^{-\tau/\mu_o} - e^{-\tau/\mu})/(1 - \mu/\mu_o), \quad \text{(A1)}$$

where τ, $\bar{\omega}_o$ and $P(\Theta)$ are the optical thickness, single scattering albedo and phase function, respectively, involving molecular and aerosol scattering. The scattering angle Θ is given by $\cos\Theta = \mu\mu_o + \sqrt{1-\mu^2}\sqrt{1-\mu_o^2}\cos(\phi - \phi_o)$, where $\mu = \cos\theta$ and $\mu_o = \cos\theta_o$. I_o is the irradiance emerging from any part of the solar disk. Strictly speaking, the solar limb darkening should be taken into account for I_o. The finite sun with limb darkening, however, yields an error less than several tenths of a percent around several degrees of the scattering angle (Box and Deepak, 1981), so that we neglect the solar limb darkening in this study. Thus, $I_o\bar{\omega}_o$ is independent of the angular coordinates and it is given to be unity. A geometrical configuration of the measurement is illustrated in Fig. A1. When the aureolemeter is aimed to a direction $(\bar{\theta}, \bar{\phi})$ against the sun's direction $(\bar{\theta}_o, \bar{\phi}_o)$, the intensity of scattered radiation derived from radiance measurements is expressed as

$$I_{obs}(\bar{\mu}, \bar{\mu}_o, \bar{\phi} - \bar{\phi}_0) = (2\pi(\cos\beta - 1))^{-1}(2\pi(\cos\alpha - 1))^{-1} \times \int_0^{2\pi}\int_1^{\cos\alpha}\int_0^{2\pi}\int_1^{\cos\beta} I(\mu, \mu_0, \phi - \phi_0) \times \cos\Theta_2 d(\cos\Theta_2) d\Phi_2 d(\cos\Theta_1) d\Phi_1, \quad \text{(A2)}$$

where α and β are the half angle of the solar disk and that of the aureolemeter's field-of-view (FOV), respectively. The other quantities are given by spherical trigonometry as follows.

$$\bar{\mu} = \cos\bar{\theta}, \quad \bar{\mu}_o = \cos\bar{\theta}_o,$$

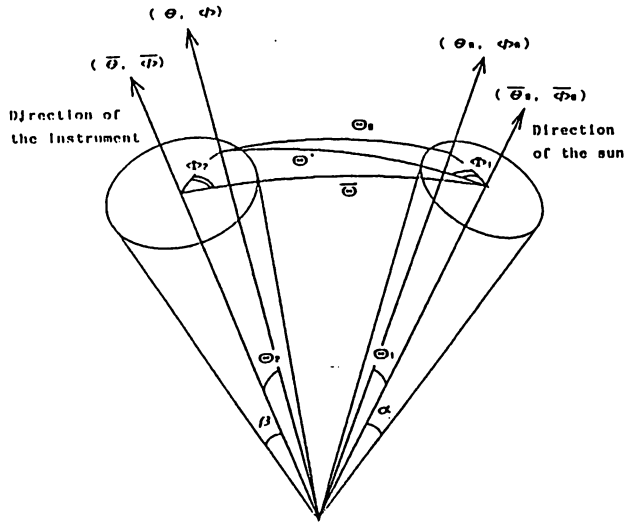

Fig. A1. The geometrical relationship among the directions of the sun ($\bar{\theta}_o$, $\bar{\phi}_o$), the aureolemeter ($\bar{\theta}$, $\bar{\phi}$), and solar radiation emerging from a point in the sun (θ_o, ϕ_o) and scattered to a point in a viewing cone of the aureolemeter (θ, ϕ). α and β are the half angle of the solar disk and that of the aureolemeter's field-of-view, respectively.

$$\mu_0 = \bar{\mu}_0 \cos\Theta_1 + \sqrt{1-\bar{\mu}_0^2}\sin\Theta_1 \sin\Phi_1,$$

$$\cos\Theta_0 = \cos\Theta' \cos\Theta_1 + \sin\Theta' \sin\Theta_1 \sin\Phi_1,$$

$$\mu = \bar{\mu}\cos\Theta_2 + \sqrt{1-\bar{\mu}^2}\sin\Theta_2 \sin\Phi_2,$$

$$\cos\Theta' = \cos\bar{\Theta}\cos\Theta_2 + \sin\bar{\Theta}\sin\Theta_2 \sin\Phi_2,$$

and

$$\cos\bar{\Theta} = \bar{\mu}\bar{\mu}_0 + \sqrt{1-\bar{\mu}^2}\sqrt{1-\bar{\mu}_0^2}\cos(\bar{\phi}-\bar{\phi}_0).$$

From Eqs. (A1) and (A2), the nominal phase function $\bar{P}(\bar{\Theta})$ obtained from the measurement is given by

$$\bar{P}(\bar{\Theta}) = I_{obs}\left(\bar{\mu}, \bar{\mu}_o, \bar{\phi}-\bar{\phi}_o\right) \times (1-\bar{\mu}/\bar{\mu}_0) \Big/ \left(e^{-\tau/\bar{\mu}_0} - e^{-\tau/\bar{\mu}}\right). \quad \text{(A3)}$$

Since the aureole measurements were made at the solar almucantar, *i.e.* $\bar{\mu}=\bar{\mu}_o$, Eq. (A3) can be replaced by the following equation:

$$\bar{P}(\bar{\Theta}) = I_{obs}\left(\bar{\mu}, \bar{\mu}_o, \bar{\phi}-\bar{\phi}_o\right) \cdot e^{\tau/\bar{\mu}_0} \cdot \bar{\mu}_0/\tau. \quad \text{(A4)}$$

After simulating I_{obs} for moderate aerosol loading with a power law size distribution, the nominal $\bar{P}(\bar{\Theta})$ was compared with the exact $P(\bar{\Theta})$ for several FOVs. The relative errors, defined as $(\bar{P}(\bar{\Theta}) - P(\bar{\Theta}))/P(\bar{\Theta})$, calculated for the wavelengths of 350 nm and 700 nm are shown in Fig. A2. The magnitude of errors is greater with larger β. $\bar{P}(\bar{\Theta})$ is

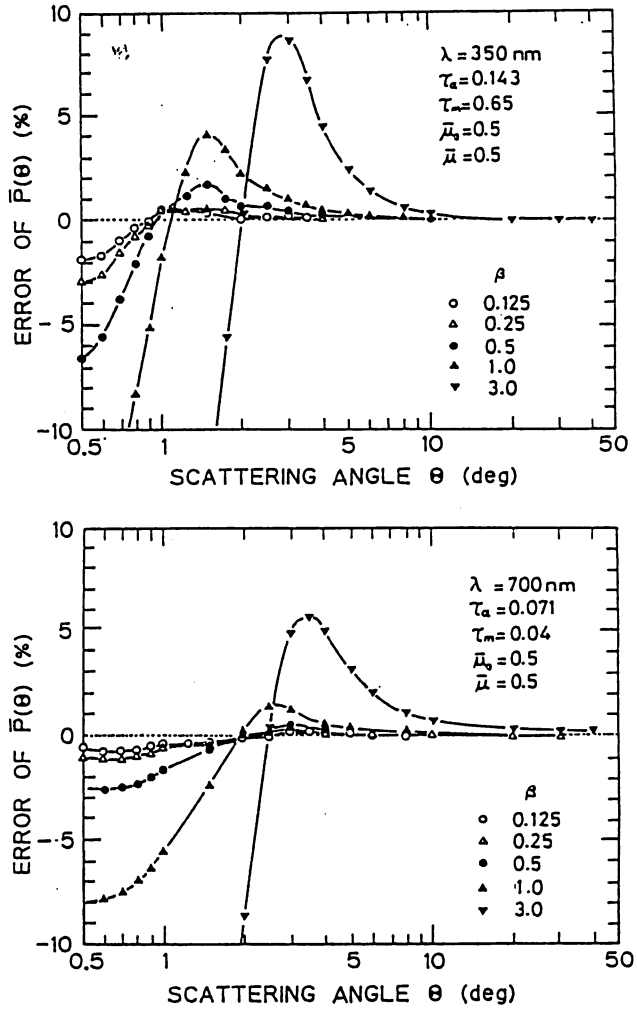

Fig. A2. Relative errors of the nominal phase function $\bar{P}(\Theta)$ against the exact one $P(\Theta)$ for λ=350 nm (upper panel) and λ=700 nm (lower panel). β is the half angle of the aureolemeter's field-of-view. The optical thicknesses of aerosols τ_a and molecules τ_m are assumed to be 0.143 and 0.65 at λ=350 nm, and 0.071 and 0.04 at λ=700 nm, respectively.

overestimated at $\bar{\Theta}$ of several degrees for any value of β, because $P(\Theta)$ increases exponentially as Θ becomes smaller at those region. On the contrary, $\bar{P}(\bar{\Theta})$ is underestimated at very small scattering angles. This is because the contribution of radiance at smaller Θ to the total radiance received by the aureolemeter becomes smaller. In other words, the finiteness of FOVs causes an apparent shift of the scattering angle from the exact one. The magnitude of such apparent shifts depends on β and the radiance distribution in the aureole region, hence being responsible for the magnitude of errors in $\bar{P}(\bar{\Theta})$. The calculations for λ=700 nm show that the influence of finite FOVs is smaller than those for λ=350 nm because the angular variation of the phase func-

tion in the aureole region at longer wavelengths becomes smaller. Results of the calculations indicate that the FOV of the instrument should be carefully determined for accurate measurements of the solar aureole.

References

Arao, K. and Y. Ishizaka, 1986: Volume and mass of yellow sand dust in the air over Japan as estimated from atmospheric turbidity. *J. Meteor. Soc. Japan*, **64**, 79–94.

Asano, S., M. Sekine, M. Kobayashi and K. Murai, 1985: Atmospheric turbidity and aerosol size distribution in winter at Tsukuba; effects of the eruption of El Chichon. *J. Meteor. Soc. Japan*, **63**, 453–463.

Box, M.A. and A. Deepak, 1981: Finite sun effect on the interpretation of solar aureole. *Appl. Opt.*, **20**, 2806–2810.

CIAP, 1975: *The natural stratosphere of 1974; CIAP Monograph 1.* Climatic Impact Assessment Program, 5.167–5.170.

Coakley Jr., J.A., R.D. Cess and F.B. Yurevich, 1983: The effect of tropospheric aerosols on the earth's radiation budget: A parameterization for climate models. *J. Atmos. Sci.*, **40**, 116–138.

Coakley Jr., J.A. and R.D. Cess, 1985: Response of the NCAR community climate model to the radiative forcing by naturally occurring tropospheric aerosol. *J. Atmos. Sci.*, **42**, 1677–1692.

Deepak, A., M.A. Box and G.P. Box, 1980: Retrieval of aerosol size distributions from scattering and extinction measurements in the presence of multiple scattering. *Remote Sensing of Atmospheres and Oceans*, Academic Press (New York), 95–113.

Fitch, B.W. and T.S. Cress, 1981: Measurements of aerosol size distributions in the lower troposphere over Northern Europe. *J. Appl. Meteor.*, **20**, 1119–1128.

Fitch, B.W. and T.S. Cress, 1983: Statial and temporal variations of tropospheric aerosol volume distribution. *J. Climate Appl. Meteor.*, **22**, 1262–1269.

Fröhlich, C. and G.E. Shaw, 1980: New determination of Rayleigh scattering in the terrestrial atmosphere. *Appl. Opt.*, **19**, 1773–1775.

Gooding, J.L., U.S. Clanton, E.M. Gabel and J.L. Warren, 1983: El Chichon volcanic ash in the stratosphere; particle abundances and size distributions after the 1982 eruption. *Geophys. Res. Letters*, **10**, 1033–1036.

Green, A.E.S., A. Deepak and B.J. Lipofsky, 1971: Interpretation of the sun's aureole based on atmospheric aerosol models. *Appl. Opt.*, **10**, 1263–1279.

Hayasaka, T., T. Nakajima and M. Tanaka, 1990: The coarse particle aerosols in the free troposphere around Japan. *J. Geophys. Res.*, **95**, 14039–14047.

Hayashida, S., and Y. Iwasaka, 1985: On the long term variation of stratospheric aerosol content after the eruption of volcano El Chichon; lidar measurements at Nagoya, Japan. *J. Meteor. Soc. Japan*, **63**, 465–473.

Hofmann, D.J. and J.M. Rosen, 1984: On the temporal variation of stratospheric aerosol size and mass during the first 18 months following the 1982 eruptions of El Chichon. *J. Geophys. Res.*, **89**, 4883–4890.

Kim, Y.J., H. Sievering, and J.F. Boatman, 1988: Airborne measurements of atmospheric aerosol particles in the lower troposphere over central United States. *J. Goephys. Res.*, **93**, 12631–12644.

Knelman, F., N. Dombrowski and D.M. Newitt, 1954: Mechanism of the bursting of bubbles. *Nature*, **173**, 261.

Knollenberg, R.G. and D. Huffman, 1983: Measurements of the aerosol size distributions in the El Chichon cloud. *Geophys. Res. Letters*, **10**, 1025–1028.

Michalsky, J.J., B.M. Herman and N.R. Larson, 1984: Mid-latitude Stratospheric aerosol layer enhancement by El Chichon; the first year. *Geophys. Res. Letters*, **11**, 76–79.

Mossop, S.C., 1964: Volcanic dust collected at an altitude of 20 km. *Nature*, **203**, 824–827.

Nakajima, T., M. Tanaka and T. Yamauchi, 1983: Retrieval of the optical properties of aerosols from aureole and extinction data. *Appl. Opt.*, **22**, 2951–2959.

Nakajima, T., M. Tanaka, T. Hayasaka, Y. Miyake, Y. Nakanishi and K. Sasamoto, 1986a: Airborne measurements of the optical stratification of aerosols in turbid atmosphere. *Appl. Opt.*, **25**, 4374–4381.

Nakajima, T., T. Takamura, M. Yamano, M. Shiobara, T. Yamauchi, R. Goto and K. Murai, 1986b: Consistency of aerosol size distributions inferred from measurements of solar radiation and aerosols. *J. Meteor. Soc. Japan*, **64**, 765–776.

Oberbeck, V.R., E.F. Danielsen, K.G. Snetsinger and G.V. Ferry, 1983: Effect of the eruption of El Chichon on stratospheric aerosol size and composition. *Geophys. Res. Letters*, **10**, 1021–1024.

Patterson, E.M. and D.A. Gillette, 1977: Commonalities in measured size distributions for aerosols having a soilderived component. *J. Geophys. Res.*, **82**, 2074–2082.

Post, M.J., 1986: Atmospheric purging of El Chichon debris. *J. Geophys. Res.*, **91**, 5222–5228.

Quenzel, H. and E. Thomalla, 1987: Remote determination of the aerosol size distribution from ground-based measurements of the solar aureole radiance. *Atmospheric radiation—Progress and prospects, Proc. Beijing Int'l. Radiation Symp. Aug. 26–30, 1986*, Ed. K-N Liou and Zhou Xiuji, Science Press (Beijing), 638–644.

Shaw, G.E., 1979: Inversion of optical scattering and spectral extinction measurements to recover aerosol size spectra. *Appl. Opt.*, **18**, 988–993.

Shibata, T., M. Fujiwara and M. Hirono, 1984: The El Chichon volcanic cloud in the stratosphere; lidar observation at Fukuoka and numerical simulation. *J. Atmos. Terr. Phys.*, **46**, 1121–1146.

Spinhirne, J.D. and M.D. King, 1985: Latitudinal variation of spectral optical thickness and columnar size distribution of the El Chichon stratospheric aerosol layer. *J. Geophys. Res.*, **90**, 10607–10619.

Takamura, T. and M. Tanaka, 1985: Some uncertainties in optical properties of aerosols estimated from light scattering measurements. *J. Meteor. Soc. Japan*, **63**, 969–974.

Tanaka, M., T. Nakajima and T. Takamura, 1982: Simultaneous determination of complex refractive index and size distribution of airborne and water-suspended particles from light scattering measurements. *J. Meteor. Soc. Japan*, **60**, 1259–1272.

Tanaka, M., T. Takamura and T. Nakajima, 1983: Refractive index and size distribution of aerosols as estimated from light scattering measurements. *J. Clim. Appl. Meteor.*, **22**, 1253–1261.

Tanaka, M., T. Nakajima and M. Shiobara, 1986: Calibration of a sunphotometer by simultaneous measurements of direct-solar and circumsolar radiations. *Appl. Opt.*, **25**, 1170–1176.

Tanaka, M., M. Shiobara, T. Nakajima, M. Yamano and K. Arao, 1989: Aerosol Optical Characteristics in the yellow sand events observed in May, 1982 at Nagasaki—Part I Observations. *J. Meteor. Soc. Japan*, **67**, 267–278.

Tanaka, M., T. Hayasaka and T. Nakajima, 1990: Airborne measurements of optical properties of tropospheric aerosols over an urban area. *J. Meteor. Soc. Japan*, **68**, 335–345.

Tanre, D., C. Deuaux, M. Herman and R. Santer, 1988: Radiative properties of desert aerosols by optical ground-based measurements at solar wavelengths. *J. Geophys. Res.*, **93**, 14223–14231.

Toba, Y., 1959: Drop production by bursting of air bubbles on the sea surface (II) theoretical study on the floating bubbles. *J. Oceanogr. Soc. Japan*, **15**, 121–130.

Toon, O.B. and J.B. Pollack, 1976: A global average model of atmospheric aerosols for radiative transfer calculations. *J. Appl. Meteor.*, **15**, 225–246.

Twitty, J.T., R.J. Parent, J.A. Weinman and E.W. Eloranta, 1976: Aerosol size distributions; remote determination from air-borne measurements of the solar aureole. *Appl. Opt.*, **15**, 980–989.

Twomey, S.A., M. Piepgrass and T.L. Wolfe, 1984: An assessment of the impact of pollution on global cloud albedo. *Tellus*, **36B**, 356–366.

Uchino, O., K. Takahashi, I. Tabata, I. Akita, Y. Okada and K. Naito, 1984: Ruby lidar observations of the El Chichon dust clouds at Tsukuba (36.1°N) and comparison with UV lidar measurements at Fukuoka (33.6°N). *J. Meteor. Soc. Japan*, **62**, 679–687.

Whitby, K.T., R.B. Husar and B.Y.H. Liu, 1972: The aerosol size distribution of Los Angels smog. *Aersols and Atmospheric Chemistry*, edited by G.M. Hidy, Academic Press (New York), 237–264.

Wigley, T.M.L., 1989: Possible climate change due to SO_2-derived cloud condensation nuclei. *Nature*, **339**, 365–367.

WMO, 1983: *Experts meeting on aerosols and their climatic effects.* WMO Rep. WCP-55, 107 pp.

Woodcock, A.H., C.F. Kientzler, A.B. Arons and D.C. Blanchard, 1953: Giant condensation muclei from bursting bubbles. *Nature*, **172**, 1144–1145.

Woods, D.C. and R.L. Chuan, 1983: Size-specific composition of aerosols in the El Chichon volcanic cloud. *Geophys. Res. Letters*, **10**, 1041–1044.

Yamamoto, G. and M. Tanaka, 1969: Determination of aerosol size distribution from spectral attenuation measuremets. *Appl. Opt.*, **8**, 447–453.

Yamamoto, G. and M. Tanaka, 1972: Increase of global albedo due to air pollution. *J. Atmos. Sci.*, **29**, 1405–1412.

走査型分光放射計による仙台上空のエアロゾルの長期モニタリング

塩原匡貴

(気象研究所気候研究部)

早坂忠裕・中島映至・田中正之

(東北大学理学部大気海洋変動観測研究センター)

1981年9月から1985年5月まで仙台市郊外において走査型分光放射計（オーリオールメータ）を用いた太陽直達光・散乱光の分光観測を行なった。観測された波長別光学的厚さと太陽周辺光の強度分布からインバージョン法によりエアロゾルの粒径分布（体積スペクトル）を求めた。

1982年に起こったエルチチョン火山の噴火前後の比較から、エルチチョン起源のエアロゾルの粒径分布を得た。その結果、エルチチョン・エアロゾルは約0.5 μmにモード半径を持つ一山分布型であり、エアロゾル気柱総量に対する影響は1983年の冬(1982年12月～1983年2月)に最大となり、それから1985年の春にかけて漸減し、ほぼ噴火以前の状態に回復している様子が見出された。

気柱総エアロゾルの体積スペクトルから、エルチチョン・エアロゾルをモデル化した体積スペクトルを差し引くことにより、仙台上空の対流圏エアロゾルの季節モデルを二山対数正規分布を用いて作成した。その結果、春季と夏季とでは、エアロゾルの体積スペクトルの特徴に大きな違いが見られた。すなわち、春季には半径約3 μmの巨大粒子モードが卓越し、一方、夏季には半径約0.2 μmのaccumulationモードが卓越している。